EVLA Memo 125
Performance Tests of the EVLA Ka-Band Receiver

Rick Perley, Bob Hayward, and Brigette Hesman
NRAO

July 21, 2008

Abstract

Sensitivity measurements performed with the Ka-band prototype receiver installed on EVLA antenna #4 show that the cold-sky zenith system temperature is between 50 and 65 K over the central 10 GHz of the passband, rising to a little over 70K at the band edges. Antenna tips show that ground spillover contributes about 22K at the vertical, while atmospheric emission rises smoothly from about 7K at 26 GHz to 12K at 40 GHz. Spillover appears to increase by about 2K for low elevation observations. Preliminary efficiency estimates were made using the quasar 3C273, and show the efficiency to be between 40 and 50%. This receiver meets the project requirements for sensitivity, despite the unexpectedly high spillover.

1 Introduction

A primary requirement for the EVLA is to provide complete frequency coverage from 1 to 50 GHz with the highest possible sensitivity. This requirement will be met by installation of eight high-performance wide-bandwidth cryogenically-cooled receivers and feeds, one of which is the 26.0 − 40.0 GHz system (Ka-band). For this band, the project requirements are to have a System Equivalent Flux Density of 760 Jy, with a system temperature (at the vertical, in clear, cold weather) of 53K, and an aperture efficiency of 39%.

We report here on the results of performance tests on the prototype Ka-band receiver system mounted in EVLA antenna #4. The parameters measured were: receiver temperature, cold-sky system temperature, noise diode temperature, ground spillover temperature, antenna efficiency, and the atmospheric opacity. All were determined at numerous frequencies chosen to span the full RF tuning range.

2 Test Setup and Observations

The test setup was similar to that utilized for the K and Q band tests reported inn EVLA Memo #103. System total power was measured at the output of the T303 UX downconverter, using the scheme schematically shown in Figure 1. For the tests made below 33.1 GHz, the converted path through the T303 module was utilized. For the higher frequencies, the direct path was utilized.

The observations were taken on 6, 9, 13, and 19 June, 2008 at the frequencies shown in Table 1. The weather conditions were ideal for all observations – clear and calm with air temperatures near 25C, and dew point near 0C. Hot and cold load measurements were done for all observations. Antenna tip observations, and raster observations of 3C273 were done for the dates/frequencies listed in the table. As the initial observations indicated that there was unexpectedly high spillover at Ka band, additional observations on 19 June at K and Q band were made on this same antenna for comparison to data taken on antenna 14 in 2005.

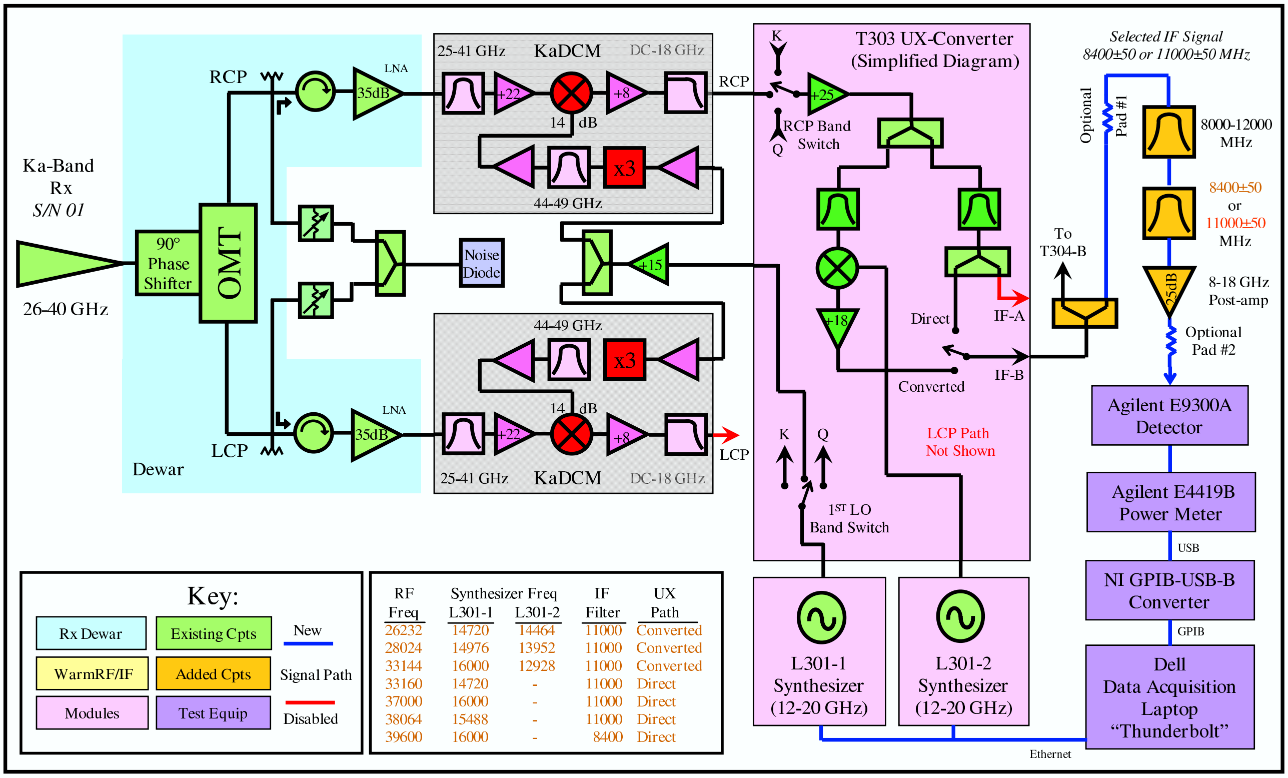

RF Freq	Synthesizer Freq L301-1	L301-2	IF Filter	UX Path
26232	14720	14464	11000	Converted
28024	14976	13952	11000	Converted
33144	16000	12928	11000	Converted
33160	14720	-	11000	Direct
37000	16000	-	11000	Direct
38064	15488	-	11000	Direct
39600	16000	-	8400	Direct

Figure 1: The setup used for determining the performance of the Ka-band receiver. The RF signals from the dewar (blue boxes) are block converted to an 8-18 GHz IF in the Ka-Band Downconverter Module (gray boxes). The 8-12 GHz portion of the IF can be selected in the T303 UX Converter (pink box) by using the 'direct' path or it can be configured to mix the signal in the 12-18 GHz portion down to the standard EVLA IF 8-12 GHz band using the 'converted' path. The output IF signal was bandpass limited by 100 MHz wide filters (gold boxes), and the power levels set with pads and post-amplifiers to give a cold-sky level of approximately -35dBm (required for a linear response by the power meter over the 10 dB power range from the cold sky to the hot loads). The power measuring system (purple boxes) comprised of an Agilent E9300A detector and E4419B power meter, whose data were recorded on a Dell Laptop (a.k.a. 'Thunderbolt') using a Labview data acquisition program. This same setup could be used to characterize the K & Q-Band systems by selecting the appropriate band switch setting. The splitter at the output of the UX Converter allows the EVLA interferometer signal path and the total power systems to operate in parallel.

3 Methodology

Determination of the system temperature, receiver temperature, spillover temperature, and atmospheric emission utilized the same 'hot-cold' load method described in EVLA Memos #85, 90, and 103.

The hot load consisted of a piece of absorber large enough to cover the horn aperture. The cold load was the same absorber, cooled with liquid nitrogen.

To monitor system gain, the internal noise diode was switched on, under computer control, as needed.

3.1 Antenna Efficiency

Antenna efficiency measurements require observations of an external source of known flux density, preferably of angular size much smaller than the antenna primary beam to minimize uncertainties in the correction for antenna beam shape. For this band, the preferred sources are the nearby

Freq MHz	Band	Date	Hot/Cold	Sky Dip	Raster
23560	K	19 Jun	Y	Y	N
26120	K	19 Jun	Y	Y	N
26232	Ka	13 Jun	Y	Y	Y
28024	Ka	13 Jun	Y	Y	Y
33144	Ka	09 Jun	Y	Y	Y
33144	Ka	13 Jun	Y	N	N
33160	Ka	06 Jun	Y	Y	Y
33160	Ka	09 Jun	Y	Y	Y
33160	Ka	13 Jun	Y	N	Y
33160	Ka	19 Jun	Y	Y	N
37000	Ka	13 Jun	Y	Y	Y
38064	Ka	13 Jun	Y	Y	N
39600	Ka	09 Jun	Y	Y	Y
39600	Ka	13 Jun	Y	Y	Y
40072	Q	19 Jun	Y	Y	N

Table 1: The observing log for the June 2008 observations.

planets Mars or Venus. Unfortunately, neither of these were in an appropriate position during the month of June, so we used the quasar 3C273, whose flux of ∼25 Jy is just adequate to provide a reasonably accurate estimate of the efficiency.

Residual antenna pointing errors are always a concern at high frequency bands, and as the interferometric 'reference pointing' observing mode could not be used to measure the pointing offset (as there was only one Ka-band antenna available), we observed in a 7 x 7 raster, with 4X oversampling, about the nominal position.

4 Results

4.1 Calibration

Calibration was accomplished using the same method as described in Memo #103. In short, the known temperatures of the hot and cold loads enable calibration of the system gain and receiver temperature, thus permitting measurement of the system power in temperature units, and separation of the internal (receiver) and external (atmospheric and spillover) contributions.

4.2 Receiver and Calibration Temperatures

The system, receiver, and noise diode temperatures of antenna #4 at Ka-band are given in Table 2.

These results show satisfactory agreement between days when the same frequencies were observed. The values for T_r and T_{cal} are very close to those measured in the lab, except at the lowest frequency. Note that the lab measurements were made without the Goretex radome – it is believed this will add 1 – 2K to the on-sky system temperatures. It is also noted there is excellent agreement for both the system and calibration temperatures between the converted path measurements taken at 33144 MHz, and the direct path measurements taken at 33160 MHz. This confirms earlier studies showing there is no loss of sensitivity due to the additional LO in the converted path.

Freq MHz	Date	T_{sys} K	T_r K	T_{cal} K	T_r K	T_{cal} K
26232	13 Jun	72	42	6.1	32	5.8
28024	13 Jun	52	21	7.6	22	7.2
33144	09 Jun	57	25	5.3	21	5.1
33144	13 Jun	55	22	5.2		
33160	06 Jun	58	25	5.2	22	5.3
33160	09 Jun	58	25	5.3		
33160	13 Jun	57	23	5.2		
33160	19 Jun	55	23	5.4		
37000	13 Jun	63	30	3.3	25	3.2
38064	13 Jun	67	32	3.3	32	3.6
39600	09 Jun	74	39	2.4	40	2.5
39600	13 Jun	75	39	2.4		

Table 2: The derived cold sky system temperatures, receiver temperatures and noise diode calibration temperatures for EVLA Antenna 4, in RCP, at Ka-band. The righthandmost pair of columns give the receiver and noise calibration temperatures as measured in the lab. Observations at frequencies below 33150 MHz were taken with the converted path through the T303 UX downconverter. Observations at the higher frequencies were taken with the direct path.

4.3 Atmospheric Emission and Spillover Temperature

Sky dips were made at all frequencies in order to determine the variation with elevation of the total system temperature. Figure 2 shows the tip curves for the data taken on 13 June.

To separate the spillover contribution from those due to atmospheric emission and cosmic background, the same simple atmospheric emission model was adopted as is described in Memo #103. In short, the observed power is assumed to be comprised of two components:

- A component which is constant with elevation, and is due to the receiver (whose contribution is independently determined through the hot/cold loads), plus a spillover contribution, originating from the ground, whose magnitude will be proportional to the ground temperature.

- A component, originating from the atmosphere and cosmic background, which follows a dependency upon elevation given by:

$$T_{sky} = T_{bb}e^{-\tau} + T_{atm}(1 - e^{-\tau}) \tag{1}$$

  where $T_{bb} = 2.75$K is the cosmic blackbody background temperature, T_{atm} is the effective radiating temperature of the atmosphere, and

$$\tau = \tau_0 \sec(z)[1 - h(\sec^2(z) - 1)] \tag{2}$$

  is the atmospheric opacity. In this expression, h is the normalized atmospheric scale height, equal to 3.1×10^{-4}. The $\sec^3(z)$ term is due to earth curvature, and is included for completeness – its influence even at the lowest elevation of 8 degrees is only $\sim$1.5%.

The tip data were thus fitted with a model described by:

$$T_{sys} = T_r + \epsilon[T_{bb}e^{-\tau} + T_{atm}(1 - e^{-\tau})] + (1 - \epsilon)T_{gnd}. \tag{3}$$

where ϵ describes the 'forward beam efficiency' – the fraction of the total power which varies with elevation according to the atmospheric emission law[1], T_r is the independently measured receiver

[1]Note that this is not the same as 'main beam efficiency'. The forward efficiency will include emission through near-in sidelobes to the main beam.

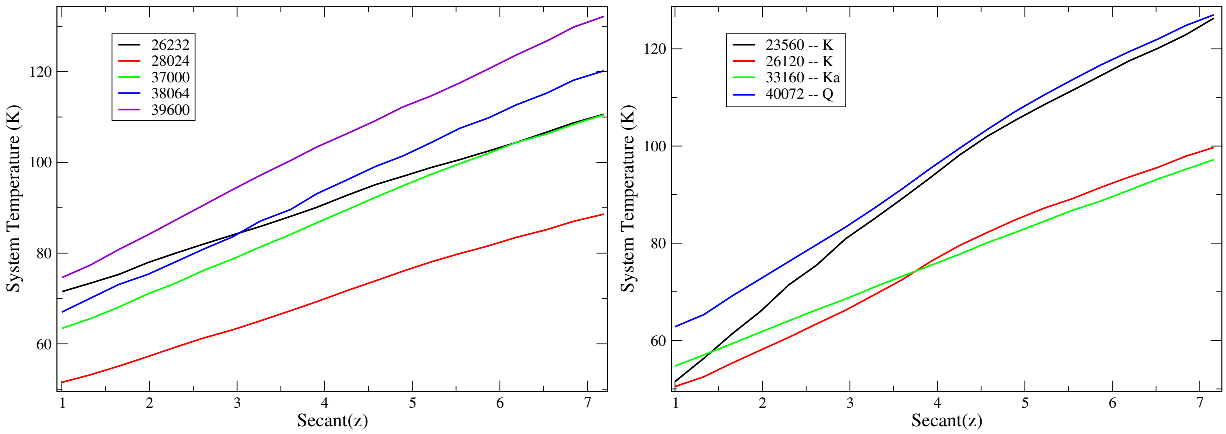

Figure 2: The two plots show the variation of system temperature with elevation. The left panel shows the profiles for various frequency in Ka-band. The right panel shows profiles from K and Q bands, for comparison.

temperature, T_{atm} is the atmospheric emission temperature, and T_{gnd} is the ground temperature. For all four days on which the observations were made, the air temperature was measured to be 297K. In these fits, the atmospheric and ground temperatures were set to 280 and 295K, respectively. The value derived by the fit for the main beam efficiency – and hence the derived spillover – is nearly independent of the atmospheric and ground temperatures. The derived opacity is inversely proportional the atmospheric temperature – the product $\tau_0 T_{atm}$ is a constant. However, the fractional error in the emission temperature is at most 5%, so the resulting maximum error in opacity is also 5%.

The assumption that the spillover temperature is independent of elevation is certainly incorrect at the level of a few degrees. We expect the largest spillover contribution to occur at elevations above ∼65 degrees, where all lines of sight from the subreflector past the edge of the primary reflector terminate on the ground, and at very low elevations, where feed spillover past the lower side of the subreflector terminates on the ground. To minimize potential variations in the spillover contribution which could bias the estimates of atmospheric opacity, we made a second fit to the data, utilizing only the tip data taken at elevations between 49 and 19 degrees. Over this range, the atmospheric curvature term can be safely ignored, and a simple $\sec(z)$ dependence of opacity employed.

The resulting residuals from both approaches are shown in Fig. 3, along with the derived opacities and spillover temperatures. The figures show that these derived values are nearly independent of the two elevation ranges used.

Comparison of the opacities and spillovers resulting from the two different approaches shows there is very little difference between them. We have elected to employ the latter method – where the fits are made using the high elevation data only – for all our data, with the results given in Table 3.

5 Comparison with K and Q Bands

Preliminary analysis of the Ka-band data indicated that the spillover contribution for this antenna was significantly higher than that determined for K and Q bands from the 2005 observations, taken on antenna #14. To determine if this apparent excess is a Ka-band effect, or is specific to antenna 4, we took hot, cold, sky, and tip data for K and Q bands on 19 June. The tip data, and the spillover residuals, utilizing the procedure described above, are shown in Fig. 4. Note that the spillover at

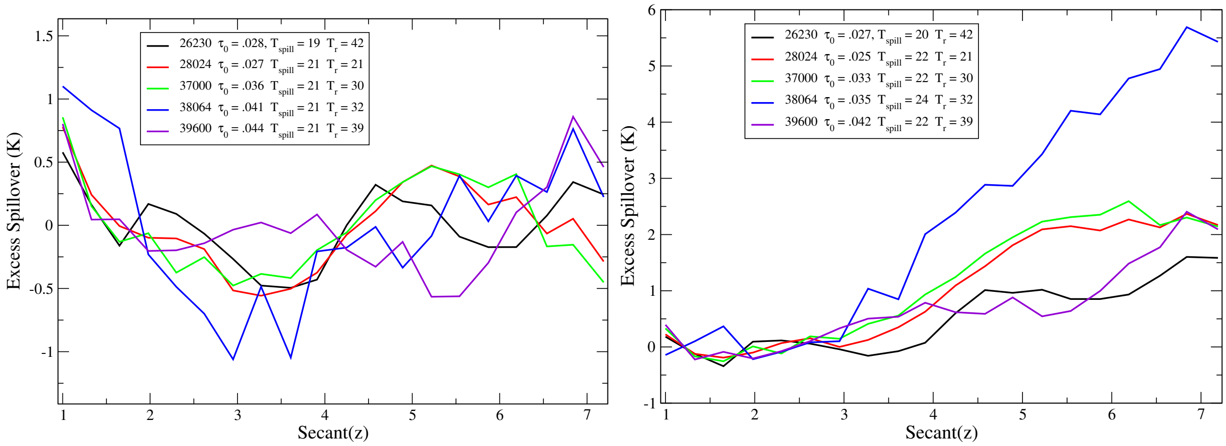

Figure 3: The residuals for two different models. In the left panel, the model was fitted to the full elevation range of data. On the right, the model was fitted to data taken at elevations above 20 degrees.

Freq MHz	τ_0	ϵ	T_r K	T_{sp} K	T_{sky} K	T_{sys} K
26232	.0267	0.932	42	20	10	72
28024	.0249	0.926	21	22	10	52
33160	.0294	0.927	23	22	11	55
37000	.0332	0.924	30	22	12	63
38064	.0354	0.920	32	24	13	67
39600	.0424	0.926	39	22	15	75

Table 3: The derived vertical atmospheric opacity,τ_0, forward efficiency, ϵ, receiver temperature T_r, spillover temperature ($T_{sp} = 295(1-\epsilon)$), antenna temperature T_{sky} due to atmospheric emission (including the 2.7K CMB) at the vertical, and total zenith cold-sky system temperature, T_{sys}.

23560 MHz (centered on the H_2O emission line) decreases markedly at very low elevation. This is unlikely to be true – direct spillover of the feed around the subreflector must see the ground at an elevation of 8 degrees. The unphysical residual shown likely indicates a failure in our emission model, most probably in the assumed value for the atmospheric scale height (2 km), or perhaps in some variation of the distribution of the water vapor in the direction of the tip. This level of detail has no effect on the deduced spillover temperature, and we have elected to not pursue more sophisticated models.

The results of the analysis are given in Table 4. From these tests, it seems clear that the vertical spillover is about 22K for this antenna at all three bands, suggesting that the higher-than expected levels are specific to this antenna.

To check on this deduction, we recovered the 2005 K and Q band data taken on antenna #14, and re-analyzed these following the same method as described above. The results are shown in Table 5.

The 2005 data show that the spillover contribution to antenna #14 is typically 15 to 17K – lower than that seen in the antenna #4 observations by 5 to 7K. As the antennas and feeds are effectively identical, the difference is more likely due to a difference in the subreflectors. An additional 7K of system temperature would occur if only 2.5% of the subreflector's reflecting surface were replaced with a blackbody absorber. While this in no way constitutes a proof that the subreflector on this antenna is defective, it does encourage a program of inspection and careful measurement.

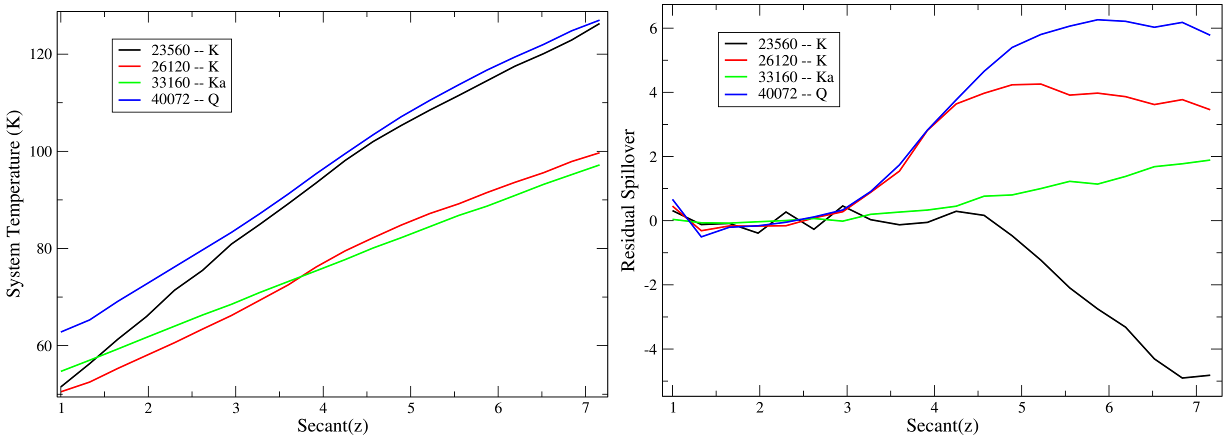

Figure 4: The tip data, and the fit residuals, for the K, Ka, and Q band data taken on 19 June on antenna #4. The high-elevation data are used to establish the atmospheric opacity. The variation of spillover with elevation is much more notable at K and Q bands than at Ka band.

Band	Freq MHz	τ_0	ϵ	T_r K	T_{sp} K	T_{sky} K	T_{sys} K
K	23560	.0665	0.930	12	21	22	52
K	26120	.0336	0.937	20	19	12	51
Ka	33160	.0294	0.927	23	22	11	55
Q	40072	.0468	0.906	20	28	16	62

Table 4: The derived vertical atmospheric opacity,τ_0, forward efficiency, ϵ, receiver temperature T_r, spillover temperature ($T_{sp} = 295(1-\epsilon)$), antenna temperature T_{sky} due to atmospheric emission (including the 2.7K CMB) at the vertical, and total zenith cold-sky system temperature, T_{sys}, for the K, Ka, and Q-band tests taken on 19 June, 2008.

6 Efficiency

The efficiency observations utilized the quasar 3C273, as the planets Venus and Mars were ill-positioned in June 2008. A 7 x 7 raster grid with 4X oversampling was used to avoid underestimating the efficiency due to pointing errors. VLBA observations of 3C273 were utilized to provide an estimate of the flux density. The provided flux densities were adjusted by the opacities derived by the atmospheric tip fits, with the results given in Table 6. Note that the 39600 MHz data were very unstable, so the resulting antenna temperature is very uncertain, and that the data taken at 33160 MHz did not use the raster grid, so the value listed in the table is very likely an underestimate.

7 Power Variations

While taking the data for this memo, we noted on numerous occasions variations in the total power on timescales of tens of seconds, typically of amplitude ∼2%, or ∼ .1dB. An example of this is shown in Fig. 5. The figure shows how the total power at 23560 MHz (K-Band receiver) changed as the antenna azimuth was rotated, back and forth, through about one-half turn while at the zenith. This plot shows that the extra noise power was reproduced at the same antenna azimuth values, suggestion a fixed origin, external to the antenna. Similar variations – but at different azimuths – were seen at 33160 MHz (in Ka band) and 40072 MHz (in Q band). The power fluctuations were seen both in the 100 MHz-wide total power, and in the T304's 1 GHz-wide total power detectors, strongly suggesting that the origin has a broad-band spectrum. The variations are not

Date	Band	Freq MHz	τ_0	ϵ	T_r K	T_{sp} K	T_{sky} K	T_{sys} K
Jun05	K	18440	.0184	0.954	23	14	8	45
Oct05	K	18440	.0223	0.957	28	13	8	49
Jun05	K	23560	.0512	0.949	15	15	17	47
Oct05	K	23560	.0605	0.952	12	14	18	44
Jun05	K	26120	.0293	0.949	19	15	11	45
Oct05	K	26120	.0373	0.956	23	12	12	48
Jun05	Q	40368	.0550	0.938	23	17	18	59
Oct05	Q	40368	.0574	0.940	23	17	17	58
Jun05	Q	43440	.0711	0.943	32	17	22	70
Oct05	Q	43440	.0718	0.932	21	20	21	61
Jun05	Q	48048	.1355	0.942	39	18	38	93
Oct05	Q	48048	.1405	0.942	58	17	37	111

Table 5: The derived vertical atmospheric opacity,τ_0, forward efficiency, ϵ, receiver temperature T_r, spillover temperature ($T_{sp} = 295(1-\epsilon)$), antenna temperature T_{sky} due to atmospheric emission (including the 2.7K CMB) at the vertical, and total zenith cold-sky system temperature, T_{sys}, for the K and Q band tests taken on EVLA antenna #14 in 2005.

Freq MHz	T_a K	τ_0	E deg	S_{3C273} Jy	ϵ
26232	2.3	.0267	28	25.9	0.50
28024	2.26	.0249	35	25.9	0.49
33144	1.80	.0291	49	24.9	0.41
33160	1.56	.0326	29	24.2	0.36
37000	1.74	.0332	40	24.0	0.41
39600	≤ 2	.0424	42	23.4	$\leq .48$

Table 6: The antenna efficiency data. The columns are: (1) Frequency in MHz, (2) Observed antenna temperature due to 3C273, (3) Vertical opacity, (4) Elevation of the observation, (5) Flux density of 3C273, adjusted for attenuation, (6) Antenna aperture efficiency.

only a function of azimuth – some of the elevation dip scans show similar variations in noise power. Antenna #4 was located at pad W9 – adjacent to the control building, technical buildings, and the ALMA test site. With the array in the 'D' configuration, there are many nearby antennas, any of which are possible origins for the observed emission.

Small changes in gain are not a serious issue to interferometry, as the correlator provides the correlation coefficient, effectively cancelling out any gain changes, provided they are resolved out temporally. Variable broad-band noise is a more serious issue, as these will reduce the correlation coefficient and – if the noise source is seen by more than one antenna – will produce an interfering signal which can confuse subsequent calibration and degrade imaging.

Further work will be needed to elucidate the origin of these variations.

8 Conclusions and Discussion

The Ka-band system meets the EVLA requirements: An efficiency between 0.4 and 0.5 easily meets the requirement of 0.38 (with further improvement likely as the optics, and antenna surface are improved), while the zenith system temperature is at, or only slightly above, the requirement of 53K.

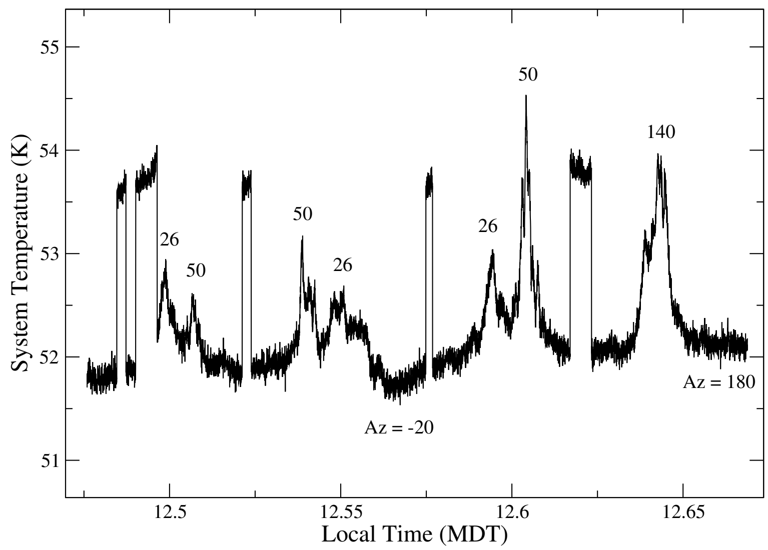

Figure 5: Showing changes in gain or, more likely, external broadband emission at 23560 MHz as the antenna was rotated in azimuth. Similar variations were seen in Ka and Q band observations. The antenna was rotated through about one-half turn, while pointed at the zenith. The annotated numbers show the antenna azimuth. The five abrupt changes in power level are due to the calibration noise diode.

There is good evidence for a small, but significant excessive spillover on antenna #4, which we could be due to a problem with the subreflector. Further tests to check this hypothesis are needed.

Occasional small variations in total system power with both movement in azimuth and elevation were observed at all three bands – for which there is some evidence is due to external broad-band emission.

Future tests which are being planned include:

- Placing the 2nd prototype receiver on an antenna known to be a good performer at K and Q bands, and repeating the tests reported here.
- Heating the subreflector by pointing at the sun, then monitoring the received power when pointing to the zenith, in an attempt to separate subreflector emission from ground spillover.
- More total power monitoring while moving the antenna in azimuth with the antenna at different elevations, in an attempt to localize the source of the external emission.
- Repeating the efficiency measurements this fall, when Venus near maximum elongation.

We thank Brian Butler and Ken Sowinski for generating the tip and raster scripts (often under short notice!), and Emmanuel Momjian for assistance in taking these data.